

Two-photon double ionization of atomic beryllium with ultrashort laser pulsesF. L. Yip,¹ A. Palacios,² F. Martín,^{2,3,4} T. N. Rescigno,⁵ and C. W. McCurdy^{5,6}¹*Department of Science and Mathematics, California Maritime Academy, Vallejo, California 94590, USA*²*Departamento de Química, Modulo 13, Universidad Autónoma de Madrid, 28049 Madrid, Spain*³*Instituto Madrileño de Estudios Avanzados en Nanociencia, Cantoblanco, 28049 Madrid, Spain*⁴*Condensed Matter Physics Center (IFIMAC), Universidad Autónoma de Madrid, 28049 Madrid, Spain*⁵*Lawrence Berkeley National Laboratory, Chemical Sciences, Berkeley, California 94720, USA*⁶*Department of Chemistry, University of California, Davis, California 95616 USA*

(Received 1 September 2015; published 5 November 2015)

We investigate the two-photon double ionization of beryllium atom induced by ultrashort pulses. We use a time-dependent formalism to evaluate the ionization amplitudes and generalized cross sections for the ejection of the $2s^2$ valence shell electrons in the presence of a fully occupied $1s^2$ frozen core shell. The relative contributions of the two-photon direct and sequential process are systematically explored by varying both pulse duration and central frequency. The energy and angular differential ionization yields reveal the signatures of both mechanisms, as well as the role of electron correlation in both the single and double ionization continua. In contrast with previous results on the helium atom, the presence of an electronic core strongly affects the final state leading to back-to-back electron emission even in the *a priori* less correlated two-photon sequential mechanism. In particular, a dominant pathway via excitation ionization through the $\text{Be}^+(2p)$ determines the profiles and pulse-duration dependencies of the energy and angle differential yields.

DOI: [10.1103/PhysRevA.92.053404](https://doi.org/10.1103/PhysRevA.92.053404)

PACS number(s): 32.80.Rm, 31.15.ac

I. INTRODUCTION

The theoretical study of the interaction of atoms and molecules with ultrashort laser pulses has grown dramatically since experimental techniques have advanced the production of nonlinear optical sources with high intensities [1–5]. More specifically, a complete understanding of double ionization processes of atomic targets by absorption of one or few XUV photons has been the subject of much theoretical work in recent years and has often advanced experimental work in this field by helping to unravel the various pathways that may exist to populate the double continuum. Because both electrons are simultaneously ejected into the continuum, these studies are expected to shed light on the role and importance of electron correlation in atoms. The simplest target, atomic helium, has seen the contribution of many theoretical treatments (see Ref. [6], and references therein) to elucidate the physical phenomena reported in the first experiments conducted with free electron laser sources (FELs) [7] and high-harmonic generation (HHG) [8,9].

Beyond helium and other purely two-electron targets, the computational effort and complexity of accurately representing heavier atoms grow as additional electrons must be appropriately accounted for. Very few reliable *ab initio* theoretical investigations are available on one-photon double ionization of multielectron targets like Be or Mg [10–12], and they are even scarcer for the two-photon absorption process [13]. From an experimental point of view, the two-photon double ionization of atoms brings the challenge of measuring a minor contribution with respect to the also present single ionization channel. Therefore it implies the necessity of coincident measurements of electrons and ions to distinguish the signal of different energetically allowed processes. Moreover, two-photon experiments require a coherent light source in the XUV region capable of controlling the polarization, wavelength, intensity, and carrier envelope phase of the laser pulse. Such

challenges have been overcome in several experimental studies and two-photon double ionization measurements are now available for neon using FEL light [14], and also for argon and krypton [15], and more recently for xenon [16] using HHG techniques to capture time-resolved images of autoionizing states.

To better understand the impact of multielectron dynamics in targets possessing more electrons than helium, we report accurate theoretical predictions on the two-photon double ionization of Be and the underlying mechanisms induced by ultrashort pulses with durations shorter than a few femtoseconds. Our first goal is to elucidate the fundamental role of electron correlation by comparison with the previous body of work for atomic helium. Both atoms share a closed s^2 shell configuration, with a 1S symmetry for the initial state, and consequently the same final-state symmetries will be reached by two-photon absorption. We thus explore the role of the $1s^2$ core in the double electron ejection from the valence shell, as well as the time scales and relative contributions from the two-photon paths [13]: nonsequential versus sequential double ionization. The nonsequential or direct process, where two photons are simultaneously absorbed to eject both electrons, can only be treated accurately when accounting for the electron correlation [17]. Correlation is expected to have a less important role in the sequential process, where one photon first singly ionizes the atom and the second photon ejects a second electron from the cation. In order to evaluate the correlation effects in both mechanisms (and as a function of pulse duration), we perform *ab initio* calculations on beryllium using an accurate description of the multielectron wave function within a time-dependent approach. For interpretative purposes, we also include the result of existing simple models to approximately reproduce the features of the sequential process and discuss their applicability to beryllium.

The presence of core electrons strongly affects the energetics of the Be atom in contrast with helium-like targets. Firstly,

the two-photon sequential process through the first excited state of the cation is energetically open at lower energies than the sequential process leaving the ion in its ground state. And secondly, the two-photon double ionization potential is much closer to the sequential limit than in helium, reducing the energy window (0.44 eV above half the double ionization potential) where only the direct process is open. In other words, observing a pure two-photon nonsequential process in double valence ionization of beryllium is only possible for relatively long-pulse durations (of the order of tens of femtoseconds). We will thus discuss the different signatures in the angle- and energy-differential double ionization probabilities of the sequential or nonsequential process, with specific interest on the associated time scales and pulse duration dependencies.

In the next section, we review the theoretical method and relevant computational details for the specific case of two-photon double ionization of frozen-core multielectron targets. In Sec. III, we discuss the differences in the role of nonsequential and sequential ionization mechanisms compared to helium, as well as how beryllium provides some unique features that can further reveal how electron correlation impacts the double ionization amplitudes that determine generalized cross sections. The results are presented in greater detail in Secs. III A and III B. The main conclusions are summarized in Sec. IV.

II. THEORY

A time-dependent treatment is required to explore the two-photon double ionization of beryllium induced by ultrashort pulses. The methodology we employ combines an accurate description of the multielectron wave function, as introduced in our previous investigations of time-independent problems on lithium and beryllium [18–20], with the time-dependent approach utilizing an exterior complex scaling (ECS)-based amplitude extraction method both initially developed for helium and detailed in Refs. [21,22]. This time-dependent formalism for frozen-core multielectron targets has recently been used to successfully describe the one-photon single and double ionization of Be in Ref. [23], where we found good agreement with previous theoretical results and available experimental data. The present study expands the work in Ref. [23] to consider two-photon processes. In the following, we provide the details for the four-electron target representation and focus on the relevant details in the implementation when taking into account the action of the ultrashort pulse. Atomic units are assumed throughout, unless otherwise stated.

A. Time-dependent four-electron wave function

The interaction of a finite pulse with the atomic target is described by solving the time-dependent Schrödinger equation (TDSE)

$$i \frac{\partial}{\partial t} \Psi(t) = H(t) \Psi(t), \quad (1)$$

where $H(t) = H + V(\mathbf{r}, t)$ is the full Hamiltonian (4) for the beryllium valence electrons plus the interaction term with the field $V(\mathbf{r}, t)$. Employing the dipole approximation in the length gauge, we describe the laser-atom interaction by $V(\mathbf{r}, t) = \mathbf{E}(t) \cdot \mathbf{r}$, where the time-varying electric field $\mathbf{E}(t)$ for a short

pulse with duration T is

$$\mathbf{E}(t) = \begin{cases} E_0 F(t) \sin(\omega t) \hat{\epsilon}, & 0 \leq t \leq T \\ 0, & \text{otherwise} \end{cases}, \quad (2)$$

where ω and E_0 are the central frequency and the maximum electric field amplitude of the pulse, respectively. We have chosen a sine-squared envelope, $F(t) = \sin^2(\pi t/T)$, to account for a finite pulse length of T with a smooth switch-on/switch-off of the field.

We write the four-electron wave function explicitly, which is essentially different from previous theoretical studies performed on double ionization of beryllium where the $1s^2$ core is treated using model potentials or pseudopotentials [13,24]. In our description, the wave function for the four electrons (omitting the spin terms) of beryllium is expanded as

$$\Psi(t) = \sum_{i,j} C_{i,j}(t) |\xi_i(r_1) Y_{l_i}^{m_i}(\Omega_1) \xi_j(r_2) Y_{l_j}^{m_j}(\Omega_2) \varphi_{1s}(3) \varphi_{1s}(4)|, \quad (3)$$

where the inner shell $1s^2$ electrons are held fixed in the expansion configurations (i.e., frozen-core approximation), and consequently, the expansion coefficients will only depend on the valence $2s^2$ electrons that will be ionized into the continuum. This description is expected to be valid because of the large energetic separation between the valence and core electrons and their role can be described by a closed-shell interaction potential. Thus the relevant Hamiltonian for the valence electrons becomes (in atomic units)

$$H = h(1) + h(2) + \frac{1}{r_{12}} + E_{\text{core}}, \quad (4)$$

where $1/r_{12}$ is the repulsion of the valence electrons and the impact of the static $1s^2$ core is accounted for in each one-body operator h ,

$$h = T - \frac{Z}{r} + 2J_{1s} - K_{1s}, \quad (5)$$

where T is the one-electron kinetic energy, the nuclear attraction is $-Z/r$ with a nuclear charge $Z = 4$, and $2J_{1s}$ and K_{1s} are the direct and exchange interactions of each valence electron with the $1s^2$ core, respectively. Because each determinant in Eq. (3) contains the same $1s$ orbital, the last term in Eq. (4) accounts for the energetic contribution of $1s^2$ core,

$$E_{\text{core}} = 2\epsilon_{1s} + J_{1s}, \quad (6)$$

where ϵ_{1s} is the orbital energy of each $1s$ electron. Since our focus is on the valence electrons, the constant core energy is subtracted off and the zero point of the double ionization energy in what follows is referenced to the ionized electrons infinitely separated from the Be^{2+} residual dication. The energetic and radial separation of the frozen $1s^2$ core electrons from the $2s^2$ shell of interest validates this approximation, which we believe should not significantly modify the valence double ionization results when compared to an unconstrained configuration interaction with active $1s$ electrons.

In order to construct the wave function with occupied inner shell orbitals as in Eq. (3) and maintain a computationally efficient and flexible description of the ionized electron dynamics at distances far beyond the nuclei, we

employ a radial basis for all electrons in a discrete variable representation with finite elements (FEM-DVR) [25], which has the advantageous property of representing one-body and two-body local potentials diagonally along radial coordinates. This requires the construction of a number of atomic orbitals out of the underlying FEM-DVR radial basis,

$$\xi_\alpha(r) = \sum_{j=1}^M U_{\alpha j} \chi_j(r), \quad (7)$$

where the radial atomic orbital basis $\xi_\alpha(r)$ is expanded in the FEM-DVR radial functions $\chi_j(r)$ via a unitary transformation matrix $U_{\alpha j}$. Since the occupied atomic orbitals have limited spatial extent, we rely on the finite element nature of the underlying radial basis only to reconstruct the orbitals in Eq. (7) over the innermost regions near the nuclei, i.e., over the radial extent of the $1s$ orbital. The key to this transformation into atomic orbitals over their spatial extent is to include the interaction of the core electrons with the outgoing valence electrons and prevent them from contaminating the double continuum wave function by populating unphysical states. In particular, this transformation permits projection of the doubly occupied $1s$ orbital from the configuration space while preserving the orthogonal complement of the removed $1s$ orbital, which significantly contributes for the first two electrons in the configurations of Eq. (3).

Beyond that region, and in particular over the radial distances necessary to describe ionization processes, the primitive FEM-DVR basis is untransformed. The main advantage here is that local potentials, particularly, the two-electron repulsion, retain their diagonal radial representation over large portions of the radial space. This framework accommodates an efficient description of the radial coordinates of the outgoing electrons while permitting a limited number of atomic orbitals to describe the core interactions with those electrons held fixed in the expansion determinants of Eq. (3).

Our representation of the innershell atomic orbitals on a double ionization grid provides an appropriate balance to accurately represent the core direct and exchange potentials that the outgoing electrons experience while maintaining flexibility and efficiency in describing the long-range dynamics far from the nuclei. It is worth remarking that, after solving the TDSE, the extraction of double ionization amplitudes from the propagated wave function $\Psi(t)$ in Eq. (3) requires the use of the same frozen-core potentials to remove accessible single ionization components at a particular final-state total energy E . In the following, we review the formalism employed to extract those amplitudes and to define the generalized cross sections for the specific problem of two-photon double ionization.

B. Two-photon double ionization amplitudes

Beyond the end of the pulse, the time evolution of the wave function, $\Psi(t > T)$, is governed only by the field-free Hamiltonian H of Eq. (4). To extract any spectral information, we first need the asymptotic form of the wave packet, i.e., to carry out an implicit integration from $t = T$ through $t = \infty$ and then Fourier transform to obtain the scattering function at a given final energy, E . As previously demonstrated in Refs. [21,22], instead of performing a numerical time

propagation long after the pulse action has ended, one can formally compute the scattering function for electrons ejected at a given total energy E by solving the time-independent Schrödinger equation using as the initial condition the time-propagated wave function at the end of the pulse, $\Psi(t = T)$. Therefore the problem can be written as the following driven equation:

$$(E - H)\Psi_{\text{sc}}^+(\mathbf{r}_1, \mathbf{r}_2) = \Psi(\mathbf{r}_1, \mathbf{r}_2, T), \quad (8)$$

where the time-propagated wave packet at the end of the sine-squared pulse (the driving term in the above equation) contains the information of all significantly populated spectral components from the action of the ultrashort pulse. This wave packet can be formally decomposed for $t > T$ as

$$\begin{aligned} \Psi(\mathbf{r}_1, \mathbf{r}_2, t) &= \psi_{\text{bound}}(\mathbf{r}_1, \mathbf{r}_2, t) + \psi_{\text{single}}(\mathbf{r}_1, \mathbf{r}_2, t) + \psi_{\text{double}}(\mathbf{r}_1, \mathbf{r}_2, t) \\ &= \psi_{\text{bound}}(\mathbf{r}_1, \mathbf{r}_2, t) + \sum_n \int d^3\mathbf{k}_n C(\mathbf{k}_n) \psi_{\mathbf{k}_n}^-(\mathbf{r}_1, \mathbf{r}_2) e^{-iE_{n,k_n} t} \\ &\quad + \iint d^3\mathbf{k}_1 d^3\mathbf{k}_2 C(\mathbf{k}_1, \mathbf{k}_2) \psi_{\mathbf{k}_1, \mathbf{k}_2}^-(\mathbf{r}_1, \mathbf{r}_2) e^{-iE_{k_1, k_2} t}, \end{aligned} \quad (9)$$

where $E_{n,k_n} = \epsilon_n + k^2/2$ and $E_{k_1, k_2} = k_1^2/2 + k_2^2/2$, and involves only free propagation with no laser field for $t > T$. The solution of the driven equation in Eq. (8) extracts the information for a given energy E from all components (bound, single, and double ionization contributions), where we shall focus on the double ionization amplitudes $C(\mathbf{k}_1, \mathbf{k}_2)$ in the present investigation. Because we are interested in the ionization components, we will use exterior complex scaling (ECS) to enforce the correct outgoing-wave boundary conditions for $\Psi_{\text{sc}}^+(\mathbf{r}_1, \mathbf{r}_2)$ (see Ref. [26] for details). Solving the driven equation with ECS extracts the second and third terms in the formal expansion of Eq. (9) at total energy E . Once we have identified the amplitudes in the asymptotic form of the scattering wave, we can separately compute them for double (or single) ionization, by employing a well-tested formalism that reduces the problem to the calculation of a simple surface integral [21,26]. The double ionization amplitude $C(\mathbf{k}_1, \mathbf{k}_2)$ for ejecting two valence electrons with momenta \mathbf{k}_1 and \mathbf{k}_2 and yielding the frozen-core Be^{2+} dication, is thus given by

$$\begin{aligned} C(\mathbf{k}_1, \mathbf{k}_2) &= \frac{1}{2} e^{i\gamma} \int \{ \phi_{\mathbf{k}_1}^{-*}(\mathbf{r}_1) \phi_{\mathbf{k}_2}^{-*}(\mathbf{r}_2) \nabla \Psi_{\text{sc}}^+(\mathbf{r}_1, \mathbf{r}_2) \\ &\quad - \Psi_{\text{sc}}^+(\mathbf{r}_1, \mathbf{r}_2) \nabla [\phi_{\mathbf{k}_1}^{-*}(\mathbf{r}_1) \phi_{\mathbf{k}_2}^{-*}(\mathbf{r}_2)] \} \cdot d\mathbf{S}, \end{aligned} \quad (10)$$

where we need to carefully choose the appropriate testing functions, $\phi_{\mathbf{k}_1}^{-*}(\mathbf{r}_1) \phi_{\mathbf{k}_2}^{-*}(\mathbf{r}_2)$, that eliminate all other components in Eq. (9) by orthogonality [26]. The individual testing functions $\phi_{\mathbf{k}}^{-*}(\mathbf{r})$ represent a continuum solution of the one-body Hamiltonian in Eq. (5) that asymptotically sees a nuclear charge of $Z = 2$. We remark that the amplitude extraction in Eq. (10) does not project onto uncorrelated final states, but rather extracts from the full solution of $\Psi_{\text{sc}}^+(\mathbf{r}_1, \mathbf{r}_2)$ only those components that place both electrons in the continuum, so long as the bound and single ionization channels are orthogonal to the testing functions (see Refs. [21,27] for more details). Thus the other role of properly accounting for the frozen-core $1s^2$ electrons is to perfectly screen the bare nuclear charge

of beryllium at long distance to account for the residual charge seen by the outgoing electron(s). Note that the γ in Eq. (10) is a volume-dependent phase that imparts no physical consequences [27].

C. Generalized differential cross sections

We employ time-dependent perturbation theory (TDPT) to define double ionization amplitudes. The propagated wave packet, after the interaction with a single pulse, is utilized to extract double ionization amplitudes over an *energy range* consistent with the bandwidth of the pulse centered on ω . Regardless of the final channel populating single or double ionized continua, one can use the first-order TDPT expressions to write exactly the one-photon absorption amplitudes as a product of the dipole matrix element from the initial to the final state and a “shape function,” $F^{2\omega}$, which is merely the Fourier transform of the pulsed radiation [21,28]. An equivalent treatment is here used for the two-photon absorption. Although the factorability of the transition amplitude is no longer strictly exact, it remains valid in the absence of states resonant with the one-photon transition [22].

The generalized cross section differential in both angle and electron ejection for a two-photon absorption process is defined as the transition rate M_{if} from an initial state i to a final state f , which is given by Fermi’s golden rule, divided by the photon flux. In the length gauge, the differential cross section is written as

$$\frac{d\sigma}{d\Omega dE_1^f dE_2^f} = \frac{8\pi^2 k_1 k_2 (\omega_{fi}/2)^2}{c^2} |M_{if}|^2, \quad (11)$$

where the transition rate involves a summation over all the eigenstates of the target:

$$M_{if} = \sum_m \frac{\langle \Phi_f^- | \epsilon \cdot \mathbf{p} | \Phi_m \rangle \langle \Phi_m | \epsilon \cdot \mathbf{p} | \Phi_i \rangle}{E_0 + \omega_{im} + \omega_{mf} - E_m + i\eta}. \quad (12)$$

Furthermore, the integral of Eq. (11) over the directions of the ejected electrons yields the single differential (energy sharing) generalized cross section.

The two-photon absorption amplitude for a finite pulse is written in second-order TDPT as

$$C^{2\omega} = \left(\frac{-i\alpha E_0}{em} \right)^2 \times \sum_m \langle \Phi_f^- | \epsilon \cdot \mathbf{p} | \Phi_m \rangle \langle \Phi_m | \epsilon \cdot \mathbf{p} | \Phi_i \rangle F^{2\omega}(\omega, \omega_{fi}, \omega_m, T), \quad (13)$$

where

$$F^{2\omega}(\omega, \omega_{fi}, \omega_m, T) = \frac{1}{2} \int_0^T dt' e^{i(\omega_{mf}-\omega)t'} \sin^2(t'\pi/T) \times \frac{1}{2} \int_0^{t'} dt'' e^{i(\omega_{im}-\omega)t''} \sin^2(t''\pi/T), \quad (14)$$

is the Fourier transform of the pulse evaluated at each transition, thus implying a double integral with an explicit m -state dependence. Nevertheless, we found that this function

can be reasonably approximated by an m -independent analytical form, $\mathfrak{F}(\omega, \omega_{fi}, T)$, which becomes exact in the long-time limit ($T \rightarrow \infty$) provided no intermediate state resonances lie within the bandwidth of the pulse (further details are given in Ref. [21]). Consequently, this approximation allows for the factorability of the time-dependent function in expression Eq. (13), and enables us to rewrite the generalized two-photon double ionization cross section as

$$\frac{d\sigma^{2\omega}}{dE_1 d\Omega_1 d\Omega_2} = \frac{8\pi^2 k_1 k_2 (\omega_{fi}/2)^2}{c^2 |E_0|^4} \frac{|C(\mathbf{k}_1, \mathbf{k}_2)|^2}{|\mathfrak{F}(\omega, \omega_{fi}, T)|^2}, \quad (15)$$

where the approximated double integral for the Fourier transform gives what has previously been referred to as the “shape function” for sine-squared pulses:

$$\mathfrak{F}(\omega, \omega_{fi}, T) = \frac{6e^{-iT(2\omega-\omega_{fi})}(e^{iT(2\omega-\omega_{fi})} - 1)\pi^4}{(2\omega-\omega_{fi})[T^4(2\omega-\omega_{fi})^4 - 20\pi^2 T^2(2\omega-\omega_{fi})^2 + 64\pi^2]}. \quad (16)$$

The sequential ionization process, in which one photon first ionizes the neutral target and the second photon ionizes the ion, implies two separate transition rates, and therefore is not appropriately described by a cross section as in Eq. (11). In fact, this expression would become singular at the energies that are resonant with each ionization threshold of the neutral in the limit of an infinitely long pulse. Nevertheless, the (generalized) formulas given here are still well-defined and maintain their connection to the nonsequential ionization threshold where the two-photon cross section is physical below these intermediate-state resonances. In addition, the generalized cross sections in Eq. (15) continue to be proportional to moduli-squared double ionization amplitudes. For the analysis that follows, we thus will use these expressions to define the cross section at any frequency to elucidate the role of the pulse length and other pulse-dependent consequences on the double ionization amplitudes.

D. Computational implementation

The valence and core electrons for beryllium in Eq. (3) are expressed radially in the transformed orbital-DVR basis of Eq. (7), while the angular coordinates of the valence electrons are expanded in coupled spherical harmonics, $\mathcal{Y}_{l_1, l_2}^{L, M}(\mathbf{r}_1, \mathbf{r}_2)$, best suited for the spherical atomic symmetry. The first two finite elements from the origin, with boundaries at 2.0 and 7.0 bohr are used to construct the atomic orbitals. Beyond that, the radial coordinate of the the valence electrons is described by the primitive FEM-DVR with 17th order in finite elements of length 8.0 bohr. The initial bound state is found by diagonalizing the field-free Hamiltonian on a grid with radial extent up to $R = 44.0$ bohr. The diagonalization is performed by using the eigenvalue problem solvers implemented in the SLEPc libraries [29,30]. The time propagation of the pulse from zero up to $t = T$ proceeds on a larger radial grid up to 180.0 bohr. To solve the driven equation we use an ECS contour beginning at $R_0 = 180.0$ bohr with two additional complex scaled elements appended with boundaries at 188.0 and 220.0 bohr. In comparison earlier calculations on helium, larger grid extents are necessary to converge the generalized cross sections, reflecting the lower ionization threshold and larger

$2s^2$ valence shell of beryllium. The TDSE was solved using a Crank-Nicholson propagation scheme with time-steps in the range of 0.25–3.00 as. For each time step in the propagation, as well as for the driven equation that defines the scattering function, we solve a system of linear equations using the Krylov solvers implemented in the PETSc libraries [31]. The pulses employed here have an intensity of 10^{12} W/cm², the same as we previously have used for helium and which is low enough to ensure the suitability of the TDPT expressions.

In comparison to our previous time-dependent treatment of the single photon double ionization of beryllium, the number of one-electron angular terms that must be included is much larger. The generalized TDCS appeared converged with up to $l_{\max} = 11$ used for each electron, substantially larger than one-photon beryllium double ionization and the two-photon double ionization of helium. This reflects the larger contribution of angular correlation in beryllium compared to helium and the accessibility of higher individual electron partial waves as more photons are absorbed. However, the total angular momentum transition from the similarly described 1S ground-state symmetry for both helium and beryllium is the same; two-photon absorption places the ionized wave function in the 1S and 1D continua in the dipole approximation.

III. TWO-PHOTON DOUBLE IONIZATION OF BE

We compute energy and angular differential generalized cross sections for two-photon double ionization of the outer shell of Be for different pulse lengths and central frequencies. We first compute the energy differential ionization yields. These are expected to show sharp profiles for long pulses when the sequential double ionization pathway is open [17]. The wide energy spectra of short pulses (of a few femtoseconds), however, smooths out these sequential peaks and may even prevent the sequential process if the pulse duration is shorter than the relaxation time of the cation [32]. The relative contribution of the sequential and the nonsequential process can be partly inferred from the energy-differential ionization yields, as shown in previous investigations in helium [6,33]. In the second part of this section, we discuss the role and signature of electron correlation captured in the generalized cross sections differential in the angle of electron ejection for a given final energy of the system.

A. Generalized cross sections versus energy sharing

The energy diagram of beryllium is shown in Fig. 1, using as zero-energy reference the double ionized species with a remaining $1s^2$ frozen core. The ground-state energy of the $2s^2$ valence electrons is $E_0 = -27.42$ eV, meaning that two-photon valence double ionization is accessible for photons of $\hbar\omega > 13.71$ eV. The energy range to observe a pure nonsequential (direct) double ionization by two photons of beryllium is very small. In fact, for energies larger than 14.14 eV, the sequential path is already open, i.e., it is possible to eject both electrons into the continuum by first ejecting an electron from the neutral atom and leaving the ion in the first excited state ($[1s^2]2p^2P^o$). Therefore there is a narrow window of 0.44 eV (14.14–13.71 eV) where direct double ionization alone will take place. This implies that the large bandwidths

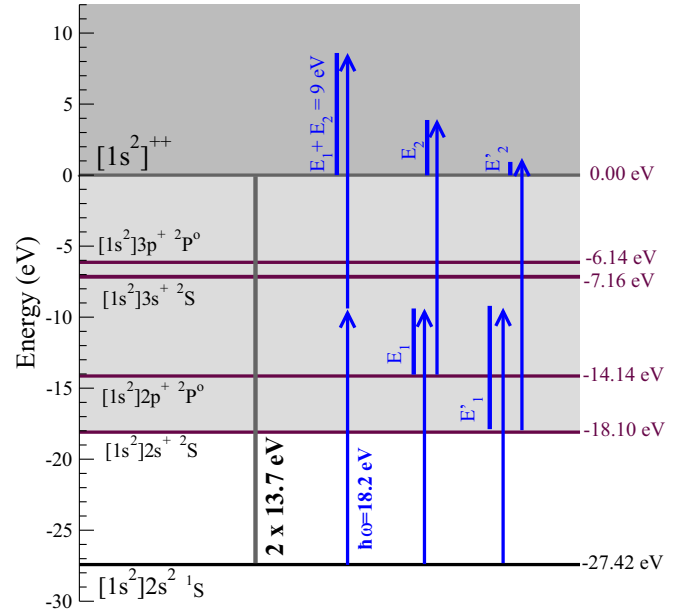


FIG. 1. (Color online) Energy level diagram of the frozen-core beryllium atom. The ground-state energy of the valence electrons is $E_0 = -27.42$ eV. Nonsequential ionization becomes the first pathway to the double continuum for $\hbar\omega = 13.71$ eV photons. Sequential ionization via the first energetically open channel occurs for photons with energy above 14.14 eV and proceeds via the $\text{Be}^+(2p)$ intermediate cation. For photons above 18.10 eV, the second sequential pathway is accessible via the $\text{Be}^+(2s)$ intermediate. The blue arrows indicate the two-photon double ionization paths accessible for a photon energy of 18.2 eV.

associated with ultrashort pulses (for instance, a pulse length of $T = 1$ fs has a full width at half maximum in energy of $\simeq 6$ eV) will always capture both the direct and the sequential components for two-photon double ionization. We omit any discussion of total ionization cross sections, because they are only well-defined in this very narrow nonsequential region.

An interesting feature of beryllium is the fact that sequential ionization first proceeds through an excited state of the ion, i.e., two-photon double ionization through excitation-ionization opens at lower energies (at 14.14 eV) than two-photon double ionization through the ground state of the ion (at 18.10 eV). Above 18.10 eV, the two-photon sequential double ionization can thus also proceed via the intermediate that leaves the remaining valence electron of the cation Be^+ in its ground-state $2s$ configuration (see Fig. 1). The opposite situation is found in He, where the absence of screening by core electrons makes excitation-ionization require more energy than ionizing the cation from its ground state. We could then infer that electron correlation is expected to be more consequential in beryllium relative to helium in the sequential region because the first photoabsorption must move both electrons, one into the continuum and one into the excited $2p$ orbital of the intermediate cation. Stated in an alternative way, the correlating configuration $2p^2$ of neutral beryllium represents a much more significant contribution to the full configuration interaction expansion of the wave function than it does in helium. Thus we can anticipate the sequential ionization of beryllium will reflect the importance of higher

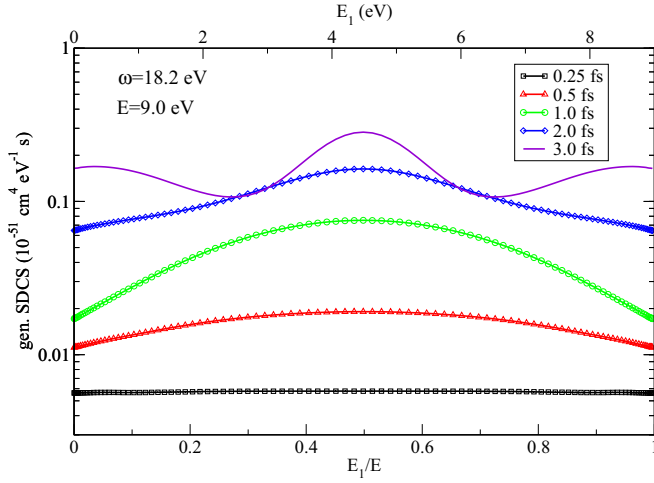


FIG. 2. (Color online) Generalized energy sharing cross section (SDCS) for two-photon double ionization of Be with $\hbar\omega = 18.2$ eV photons for various pulse durations. The excess energy above the double ionization threshold is $E = 9.0$ eV. A pair of sequential peaks near equal energy sharing $E_1/E = 0.5$ via the excited $\text{Be}^+(2p)$ intermediate is unresolved by these bandwidth-limited pulses. Longer pulses do begin to resolve the signature of helium-like sequential ionization appearing at extreme energy sharings.

angular momenta correlating configurations in the sequential region with those processes identified by this intermediate state resonance.

Regardless of the atomic target under study, for an infinitely long pulse a sequential process is expected to manifest in the single differential (generalized) cross sections (SDCS) as singularities centered at the excess energy of each electron [17]. When using finite pulses those peaks undergo a Fourier broadening together with the energy bandwidth of the pulse. By decreasing the pulse duration the sequential peaks are eventually washed out as demonstrated in helium [34]. The disappearance of the sequential peaks can be related to the Fourier broadening of the pulse or to the time required for the sequential process to take place. Only a further analysis of the angular distributions can confirm its origin. In Figs. 2 and 3, we plot the SDCS, which show the variation of the double ionization amplitudes with respect to the energy sharing between the two ionized electrons. Note that we choose to plot the SDCS as a function of energy sharing for a fixed total final energy ($E = E_1 + E_2$), instead of fixing the energy of one of the electrons and plot the SDCS as a function of the energy of the second one. The latter would lead to asymmetric profiles, while we obtain SDCS that are symmetric functions respect to 50% energy sharing, better reflecting the fact that both ejected electrons are indeed indistinguishable.

We first chose a central energy for the pulse of $\omega = 18.2$ eV. Figure 2 displays the SDCS (in units of $\text{cm}^4 \text{s eV}^{-1}$) for a fixed excess total energy of $E = 9.0$ eV for the electrons to carry away, corresponding to the maximum double ionization probability for the pulse. The lower x axis is labeled with the energy sharing and the corresponding absolute energy E_1 of the electron is shown on the upper x axis. At $\omega = 18.2$ eV, sequential ionization can only proceed via the ground ($\omega > 18.1$ eV) and the first excited state ($\omega > 14.14$ eV) of the ion.

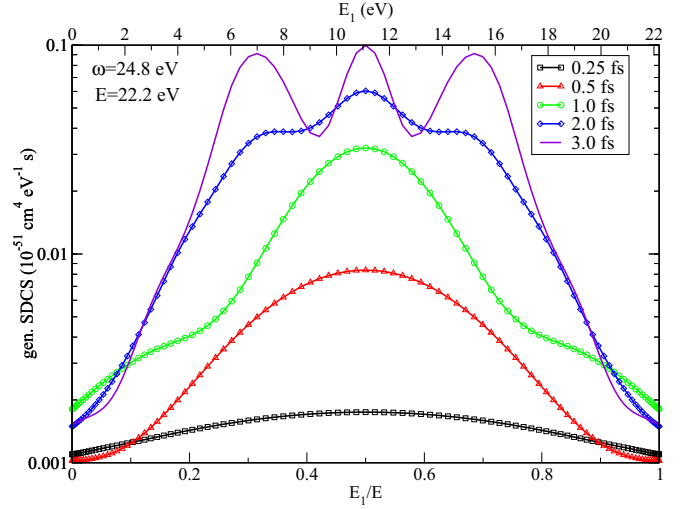


FIG. 3. (Color online) Same as Fig. 2, but with $\hbar\omega = 24.8$ eV photons. The excess energy above the double ionization threshold is $E = 22.2$ eV.

Direct and sequential two-photon paths are represented with arrows in Fig. 1. Below we present simulations performed with different pulse durations, from 250 as up to 3 fs.

The effect of increasing the pulse length results in a larger magnitude of the ionization amplitudes, as well as an enhanced resolution of the signatures of the sequential process. In principle, we would expect to observe two pairs of peaks [6], one pair associated with the sequential process via the $\text{Be}^+(2p)$ and the other pair with the sequential process via the $\text{Be}^+(2s)$, i.e., electrons ejected at $E_1 = E_0 - \epsilon_{2p} + \hbar\omega = 4.92$ eV and $E_2 = \epsilon_{2p} + \hbar\omega = 4.06$ eV for the first pair of peaks and electrons ejected at $E'_1 = E_0 - \epsilon_{2s} + \hbar\omega = 8.88$ eV and $E'_2 = \epsilon_{2s} + \hbar\omega = 0.1$ eV for the second pair. However, these signatures actually appear smoothed out, since we are using ultrashort pulses. Moreover, because the energy level of the first energetically open excitation-ionization resonance via the $\text{Be}^+(2p)$ lies almost exactly halfway between the ground-state energy E_0 of the valence electrons and the double ionization threshold, the pair of sequential ionization peaks that first appear corresponding to energies E_1 and E_2 are separated by $E_0 - 2\epsilon_{2p} = 0.86$ eV. This energy spacing is smaller than the energy bandwidth of the longest few-femtosecond pulse considered here ($\Delta\omega \sim 1.4$ eV for a 3 fs pulse). Consequently, the 0.86 eV energy gap is not resolved and the first pair of expected peaks becomes a single central peak in the SDCS in Fig. 2. Only pulse lengths larger than 15 fs would resolve the double peak structure for the sequential process via the $\text{Be}^+(2p)$. The signature associated with the sequential ionization via the $\text{Be}^+(2s)$, on the other hand, appears in the edges of the SDCS and is observed as “wings” in the SDCS in Fig. 2. Those wings are increasingly visible for the longest pulses plotted, 2 and 3 fs and are unapparent in shorter pulse lengths.

It is, however, noticeable that the signature for both sequential processes (central peak and wings) is only distinct for durations larger than 1 fs. One could then ask if the durations at which the peaks start to build up are associated with the time needed for the sequential ejection to take place

(equivalently stated, as relaxation times for the ion after the sudden removal of an electron) or are they nothing more than the result of a spectral broadening effect. *A priori*, an equivalent study for the helium atom would be the absorption of two 58 eV photons (energy right above the two-photon sequential threshold via the ground state of the ion). In that case, we observed that the sequential peaks started to show up at much shorter pulse lengths, $T \simeq 300$ as [34]. However, for He the energy spacing between those sequential peaks is $E_0 - 2\epsilon_{n=1}(\text{He}^+) = 30$ eV and, therefore, we cannot yet answer the question if the pulse length dependence is related at all to any time scale due to the sequential ejection itself or to spectral phenomena.

We thus compute the SDCS for a higher photon energy, 24.8 eV, for which electrons are ejected for each sequential process with a larger energy gap among them. Figure 3 shows the SDCS for pulses with different lengths, all centered at $\hbar\omega = 24.8$ eV, and leaving the outgoing electrons with an excess total energy of $E = 22.2$ eV to share. The features of sequential ionization associated with the $\text{Be}^+(2p)$ and $\text{Be}^+(2s)$ intermediate states, both located nearer to equal energy sharing appear more prominent at shorter pulse lengths compared to the results found at a central frequency of 18.2 eV of Fig. 2, as the spectral bandwidth of the pulses becomes less encompassing of the total excess energy available to share. In other words, the smaller energy gap between the ejected electrons seems to be the only reason why longer pulse durations are required in Be than in He in order to uncover the sequential peaks for the double ionization of the valence electrons. The consequence of the smaller energy gap between the ionic states in Be is also seen when comparing Figs. 2 and 3, in the behavior of the SDCS in the energy sharing region between sequential peaks.

As shown in previous works in helium [6,33], the generalized SDCS in the nonsequential region remain independent of the pulse duration, while the sequential peaks indefinitely grow with pulse duration. This is the case, as long as the pulse duration is long enough to resolve in energy the contributions from the different sequential processes. In the calculations presented here, this limit is only reached for pulses longer than 2 fs and confirmed by the sequential model in the lower panel of Fig. 4. For shorter pulse durations, distinguishing direct from sequential double ionization is no longer meaningful. Note that the energy width of the outer sequential peaks via the ground state of the ion have reach the width dictated by the electronic structure of the target itself. Even in the long-time limit, the sequential peaks have a finite bandwidth [17].

In Fig. 3, we also observe that for this higher photon energy new pathways for sequential ionization, via the intermediate cation now leaving the bound electron in $\text{Be}^+(n=3)$ (levels also plotted in Fig. 1), are accessible via the first photon. The signature of this excitation-ionization process becomes slightly observable in the extreme energy sharing wings of the 3.0 fs pulse of Fig. 3. This contribution, from the sequential processes through higher ionization thresholds, is noticeably smaller than the signatures for the double ionization via the $\text{Be}^+(2p)$ and $\text{Be}^+(2s)$. A similar trend was found for the helium atom, where it was observed that the sequential channel involving the ground state $\text{He}^+(1s)$ is around two orders of magnitude more intense than sequential double ionization

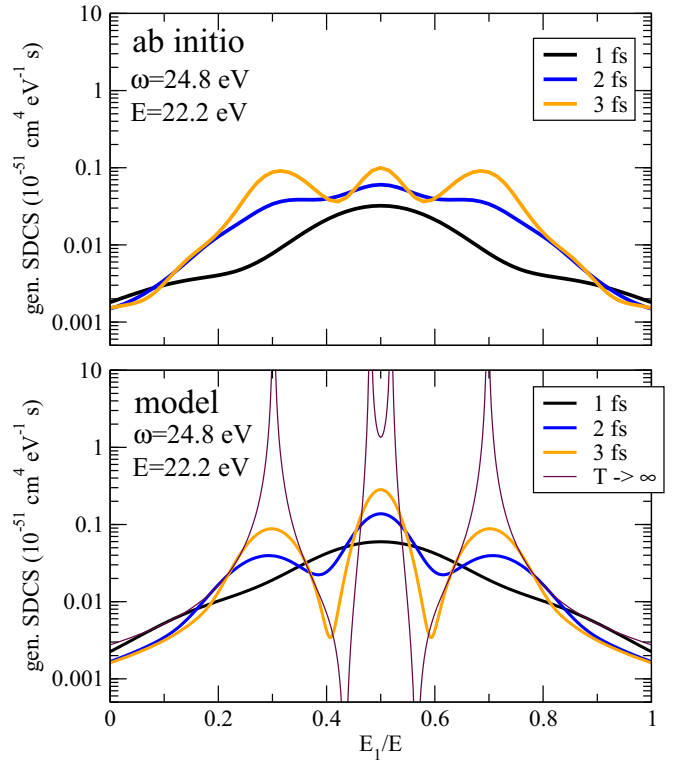


FIG. 4. (Color online) Longer pulse duration results of Fig. 3 with $\hbar\omega = 24.8$ eV photons (upper panel) along with sequential model results from Eq. (17) (lower panel).

through excitation ionization. In the present work, we see that the relative magnitude of the first two pairs of peaks are actually comparable, regardless the photon energy investigated. As the contributions of those energetically distant correlating configurations diminish in relative importance, we expect more disparate ratios in the relative sequential peak heights.

At this point, in order to elucidate how independent each photoejection is for the different sequential processes of beryllium, we consider a simple sequential model [6,34]. Briefly, the amplitude for a two-photon transition is simplified from the formal time-dependent perturbation theory expression by assuming an *uncorrelated* final-state symmetrized product of Coulomb waves and approximating the intermediate state as a the product of a bound state of the singly ionized target and a Coulomb function of the residual singly charged ion. A full derivation of the model can be found in Ref. [34], but the relevant key finding from employing this model is that the features of the energy sharing cross section can be predicted for the lowest accessible sequential peaks of helium with surprising quantitative accuracy compared to the full calculation. Below, we adapt this sequential framework from helium to beryllium, where as before, we assume that (1) the final state can be represented as an antisymmetrized product of continuum and bound states of the intermediate ion by ignoring final-state correlation and (2) screening effects by the other bound valence electron of the intermediate cation can also be neglected. Using these approximations, we can model the energy sharing cross section as antisymmetrized products of sequential single-ionization amplitudes for the two most

significant pathways involving the $2s$ and $2p$ intermediate states of Be^+ . The SDCS for beryllium is thus modeled as

$$\begin{aligned} \frac{d\sigma^{\text{seq}}(T)}{dE_1} \approx & \left(\frac{32}{T}\right)^2 \frac{1}{4\pi\hbar} \left| \sqrt{\sigma_{2p}^{\text{Be}^+}(E_2)\sigma_{2p}^{\text{Be}}(E_1)G(\alpha_{1,2p},T)} \right. \\ & + \sqrt{\sigma_{2p}^{\text{Be}^+}(E_1)\sigma_{2p}^{\text{Be}}(E_2)G(\alpha_{2,2p},T)} \\ & + \sqrt{\sigma_{2s}^{\text{Be}^+}(E_2)\sigma_{2s}^{\text{Be}}(E_1)G(\alpha_{1,2s},T)} \\ & \left. + \sqrt{\sigma_{2s}^{\text{Be}^+}(E_1)\sigma_{2s}^{\text{Be}}(E_2)G(\alpha_{2,2s},T)} \right|^2, \quad (17) \end{aligned}$$

where $G(\alpha_{i,n}T)$ is the result of making the rotating wave approximation and integrating the interacting field over time,

$$G(\alpha, T) = \frac{1}{2} \int_0^T dt' e^{i\alpha t'} F(t) \times \frac{1}{2} \int_0^{t'} dt'' e^{-i\alpha t''} F(t), \quad (18)$$

and has a simple analytical form for sine-squared envelopes, $F(t) = \sin^2(\pi t/T)$. The excess energy parameter in G is given by $\alpha_{i,n} = (E_0 + \hbar\omega - E_i - \epsilon_n)/\hbar$ for the energy of either outgoing electron E_i and the corresponding ionization threshold energy ($n = 2s$ or $2p$). Also, $\sigma^{\text{Be}}(E_i)$ and $\sigma^{\text{Be}^+}(E_i)$ refer to the single-photon photoionization cross sections of beryllium [35] or beryllium cation [36,37], respectively, with intermediate states of $\text{Be}^+(2s)$ or $\text{Be}^+(2p)$. Each distinct photoionization amplitude is being approximated as the modulus square-root of the corresponding one-photon cross section, and it includes four terms total: a pair of direct and exchange terms for each of the $2p$ and $2s$ intermediate states of the Be cation, respectively.

This is thus a sequential model where we are neglecting any correlation in the two-step process and in the final states. In Fig. 4, we show the comparison of the model output (lower panel) with the full calculation (upper panel) for 24.8 eV photons at the three longest pulse lengths previously considered. We have also included the result of the model for an infinitely long-pulse duration. The model does predict the profiles for the SDCS with good agreement compared to the *ab initio* data for the position of the peaks and of the valleys resulting from the interference between terms coming from the $2s$ and from the $2p$ transitions in Eq. (17). It should be mentioned that the model presents less quantitative consistency as the pulse length increases than similar comparisons carried out for helium. Indeed, the proportionality constants of Eq. (17) assume a pure s to p transition for which the asymmetry parameter β equals 2 and is independent of energy. We have verified that the asymmetry parameter from the $2p$ state of Be^+ is relatively constant with respect to energy, and for simplicity ignore the angular dependence associated with this p to $s + d$ transition in order to apply this sequential model for a qualitative comparison of the energy sharing.

For Be, the model substantially underestimates the signal for the outer pair of sequential peaks (those for which the $\beta = 2$ asymmetry parameter is appropriate). This, perhaps, is most likely due to the absence of the phase information between the individual photoionization events considered in this simple model, which is sacrificed by the approximation of these amplitudes as the square root of the corresponding cross section values. This limitation is also suspected of slightly shifting the model peak locations of the secondary peaks relative to their anticipated values dictated by energy

conservation. Despite the simplicity of the model, however, the general features of the energy sharing cross section and their behavior as the pulse length is increased are fairly well represented.

We mention that a quantitatively correct extension of this sequential model warrants a full discussion that will be the subject of a future publication.

B. Angular distributions

We now examine the angular distributions of the ejected electrons with respect to the light polarization direction, i.e., the (generalized) triply differential cross sections for two-photon double ionization of beryllium. For better comparison, we present the results normalized to their largest magnitude for each energy sharing, recalling that the double ionization amplitudes increase without bound as the pulse duration is lengthened above the sequential threshold. We chose three energy sharings, 30%, 50%, and 90%, for which the two photon central frequencies previously considered, 18.2 and 24.8 eV, a sequential peak is always placed near to one of them.

Figure 5 presents the angular distributions for two-photon double ionization for pulses centered at 18.2 eV (left panels) and 24.8 eV (right panels). We plot the angular distribution of one electron in the plane containing the other electron fixed along the polarization direction (taken to be the horizontal axis in the following figures). The fixed electron carries away the energy sharing indicated in each panel: a total $E = 9.0$ eV excess energy available for the 18.20 eV pulse

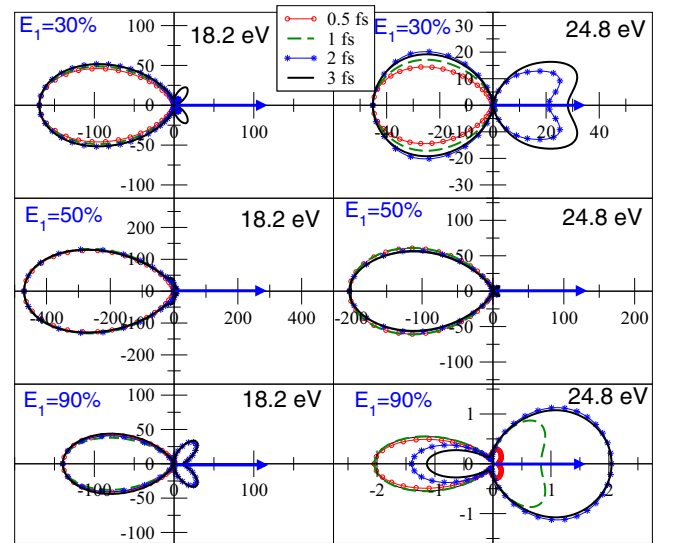


FIG. 5. (Color online) Electron angular distributions for electron 1, in the plane containing the polarization direction (horizontal) and the direction of ejection of electron 2 along the polarization ($\theta_1 = 0^\circ$). Left panels correspond to a pulse centered at 18.20 eV and an excess of energy of 9.0 eV to be shared among electrons. Right panels correspond to a pulse centered at 24.8 eV and an excess of energy of 22.2 eV. Each row corresponds to a given energy sharing (30%, 50%, and 90%) as labeled. Results have been normalized to the largest magnitude cross section of the different pulse lengths for each energy sharing. The numerical scale on the axes are reported in units of $10^{-55} \text{ cm}^4 \text{ s eV}^{-1} \text{ sr}^{-2}$.

and $E = 22.2$ eV for the 24.8 eV pulse, in correspondence with Figs. 2 and 3. The pulse lengths in every panel range from 0.5 fs to 3.0 fs.

Examination of the results at 30% energy sharing for both central energies, reveals a feature already exhibited in helium [22,34]: as the pulse duration increases the angular distribution for one electron becomes less sensitive with respect to the ejection direction of the other electron. Although more noticeable for the 24.8 eV pulse, the shorter the pulse length, the closer to a back-to-back emission of the electrons, or equivalently, when both direct and sequential two-photon ionization paths are open, the relative contribution of the direct process becomes larger for the shortest pulses.

For 50% energy sharing, we would expect to be also revealing the uncorrelated behavior of a sequential process as we increase the pulse duration, since we have the broadened sequential peaks via excitation ionization. This is quite distinct from He, where direct two-photon ionization dominates at 50% energy sharing, and an almost perfect back-to-back emission is found regardless the pulse duration. In the present case, we thus could expect an uncorrelated angular distribution, i.e. a product of two independent single-photon transitions. However, the results at equal energy sharing in Fig. 5, for both 18.2 and 24.8 eV pulses, appears to be dominated by back-to-back ejection regardless of the pulse length, and exhibits no signature of an uncorrelated sequential ionization process, despite the fact that the dominant sequential peak via the $\text{Be}^+(2p)$ intermediate lies on either side of this energy sharing midpoint less than 0.5 eV away. There is a large contribution from the sequential process even in the long-time limit, as shown in the model plotted in Fig. 4. Moreover, the ionization yield at 50% energy sharing, as shown in Figs. 2 and 3, does follow the expected enhancement for the sequential process. The highly correlated electron emission found at 50% energy sharing, where the sequential process undoubtedly dominates is thus due to the correlation in the final state since both electrons, even in a sequential process, are being ejected with the same exact energy.

The angular distributions at 90% energy sharing, mostly corresponding to the sequential ionization via the $\text{Be}^+(2s)$ intermediate, show the most change for pulse duration and energy. As explained in the previous section, at 90% for the 18.2 eV pulse, we are expecting a larger contribution from the sequential process for pulse durations larger than 1 fs, which is when the TDCS shows small lobes in the direction of ejection of the first electron, although the distributions are still mostly dominated by the back-to-back emission. For the 24.8-eV pulse, the energy difference between the energies imparted to each electron is larger, and we thus find a more uncorrelated behavior typical of the sequential electron ejection.

A remarkable feature is the fact that now both electrons seem to escape following the same direction, which can be understood in terms of a post-collision interaction effect [38]. The same behavior was found in helium for unequal energy sharings when several sequential paths are open. In this case, instead of explaining the angular distributions as a function of the energy sharing of the electrons, it is more convenient to think of the energies at which the electrons escape as a consequence of the angle that they follow when

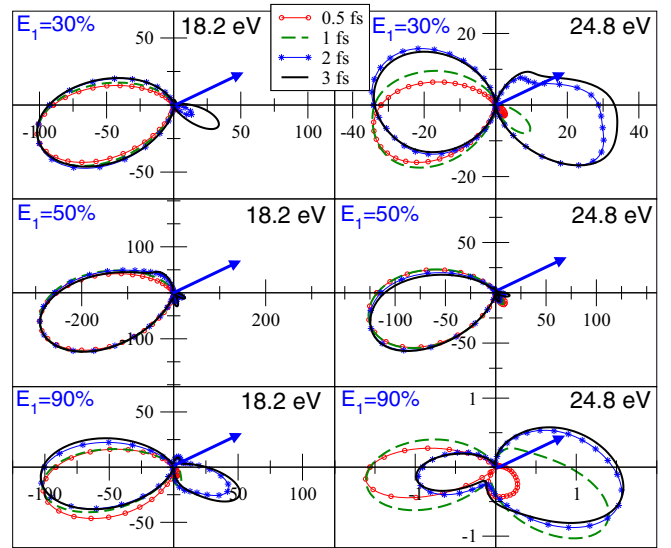


FIG. 6. (Color online) Same as Fig. 5, with the fixed electron now directed at $\theta_1 = 30^\circ$ relative to the polarization direction. The numerical scale on the axes are reported in units of $10^{-55} \text{ cm}^4 \text{ s eV}^{-1} \text{ sr}^{-2}$.

ejected. When electrons are sequentially ejected with the same angle with respect to the light polarization direction, post-collision interactions may be relevant, resulting in a fast and a slow electron and, thus an unequal energy sharing. However, when electrons are ejected in different directions, for instance back-to-back, they feel a different effective charge and leave the atom with lower energies, with an equal energy sharing. This same post-collision interaction argument can explain why at 18.2 eV the electrons leave the atom with higher correlation than at 24.8 eV. The more distinct the energies of the electrons sequentially ejected the less correlated emission, as demonstrated when comparing the TDCS for both energies in all TDCS shown in Figs. 5 and 6.

In Fig. 6, we plot the same energy sharings and excess energies as in Fig. 5, but with a different direction of ejection of the fixed electron with respect to the light polarization, $\theta_1 = 30^\circ$. More uncorrelated behavior of the ejected electrons is again shown for pulse durations larger than 1 fs in both unequal energy sharings considered. The depletion of the ionization yield when both electrons are ejected in the same direction is now more obvious for both central frequencies at 30% and 90% energy sharings (first and last rows in Fig. 6). As in the previous figure, at $E_1/E = 50\%$ energy sharing, the angular distributions again appear dominated by the correlated dynamics of equal energy sharing and much less sensitive to the pulse duration as compared to the asymmetric energy sharings, even if the SDCS clearly shows the sequential character of increasing with the pulse length. The unique case of a sequential process enhancement that produces angular distributions that appear more correlated as a consequence of lying near equal energy sharing distinguishes two-photon ionization of beryllium from helium.

In summary, in contrast with helium, the energetic similarity of the exiting electrons in Be via the first sequential ionization process produces angular patterns that appear highly

correlated and insensitive to the pulse duration. This observation indicates that sequential ionization producing photoelectrons with nearly the same kinetic energy renders an independent particle model less able to accurately represent what final-state correlation requires when the electrons move with nearly the same kinetic energy. The resulting angular distributions in these cases appear to bear the signature of direct ionization sensitive to correlation in the final state rather than sequential ionizations which leave the electrons energetically distinct, as in the upper and lower panels of Figs. 5 and 6.

IV. CONCLUSION

We have presented energy and angle-differential theoretical results for double ionization of the valence electrons of beryllium by two-photon absorption. The symmetry of the overall process in beryllium parallels that of helium, but we have found substantial differences in the behavior of the double ionization amplitudes for sequential ionization via the first sequential threshold. This difference is due to the mechanism proceeding via the first excited state of the intermediate of the excited-state cation $\text{Be}^+(2p)$, which is distinct in both the close proximity of this energy level to the ground state as well as in the symmetry of this state when compared to the ground state intermediate $\text{He}^+(1s)$ in helium sequential ionization. Further, in beryllium, the energetics of the process involving the $2p$ intermediate of Be^+ require that a sequential two-photon ionization via this intermediate produces photoelectrons with outgoing kinetic energies separated by less than 1 eV, and thus highly correlated in energy sharing.

The consequences of this energetic similarity imply that using an independent particle model to describe the angular distributions does not fully capture the final-state dynamics that produces predominantly back-to-back photoejection patterns reminiscent of correlated processes such as single-photon double ionization and nonsequential (direct) two-photon double ionization. This is in stark contrast to helium where the sequential process can be very well modeled by viewing the two-photon absorption at the sequential peaks as the product of two independent photoionization events because the continuum electrons are well-separated in energy by virtue of the intermediate energy level.

Though the first sequential threshold in beryllium is distinct in character (i.e., involving excitation-ionization) compared to helium in the intermediate cation produced after the first photoabsorption, at slightly higher photon energies the analogous process via the ground state intermediate $\text{Be}^+(2s)$

opens, resulting in a second pair of sequential peaks whose energy separation is larger, and therefore less correlated in the final state. Examination of the angular distributions corresponding to this sequential process reveals much more commonality with the behavior of helium in two-photon ionization at the sequential peak energy sharings. There, the process of ionization does appear to be much better modeled by two independent photoionization events.

The simple uncorrelated final-state model employed here which better describes the heliumlike transitions producing energetically distinct photoelectrons in two-photon absorption also hints at the limitations that arise from ignoring the interference terms between two competing sequential ionization pathways, as evidenced in the energy-sharing cross section of Fig. 4. While the model does successfully predict the location and bandwidth-limited spectral resolution of the sequential peaks fairly well, for longer duration pulses, this approximation qualitatively underestimates the double ionization amplitude between the central and heliumlike sequential peaks and is much less quantitatively accurate at describing the relative peak heights than when applied to the simpler helium atom. Because the beryllium atom features substantially more important contributions from the lower few correlating configurations than does helium, the phase information between sequential pathways must seemingly be more important to retain in order to better model the *ab initio* results.

ACKNOWLEDGMENTS

This material contains work performed at Lawrence Berkeley National Laboratory supported by the US Department of Energy Office of Science, Office of Basic Energy Sciences, Division of Chemical Sciences Contract DE-AC02-05CH11231, and work at the University of California Davis supported by US Department of Energy Grant No. DESC0007182. Work at Cal Maritime is supported by the National Science Foundation, Grant No. PHY-1509971. Work at the Autónoma de Madrid was supported by the Advanced Grant of the European Research Council XCHEM 290853, the European grants MC-ITN CORINF and MC-RG ATTOTREND FP7-PEOPLE-268284, the European COST Action XLIC CM1204, the MINECO Project No. FIS2013-42002-R and the ERA-Chemistry Project PIM2010EEC-00751. We acknowledge computer time at the Centro de Computación Científica CCC-UAM and MareNostrum from Barcelona Supercomputing Center.

-
- [1] Matthias F. Kling and Marc J. J. Vrakking, Attosecond electron dynamics, *Annu. Rev. Phys. Chem.* **59**, 463 (2008).
 - [2] Katsumi Midorikawa, High-order harmonic generation and attosecond science, *Jpn. J. Appl. Phys.* **50**, 090001 (2011).
 - [3] Lukas Gallmann, Claudio Cirelli, and Ursula Keller, Attosecond science: Recent highlights and future trends, *Annu. Rev. Phys. Chem.* **63**, 447 (2012).
 - [4] Christoph Bostedt, Henry N. Chapman, John T. Costello, José R. Crespo López-Urrutia, Stefan Düsterer, Sascha W. Epp, Josef Feldhaus, Alexander Föhlisch, Michael Meyer, and

Thomas Möller, Experiments at FLASH, *Nuclear Instruments and Methods in Physics Research Section A: Accelerators, Spectrometers, Detectors and Associated Equipment* **601**, 108 (2009).

- [5] Joachim Ullrich, Artem Rudenko, and Robert Moshhammer, Free-electron lasers: New avenues in molecular physics and photochemistry, *Annu. Rev. Phys. Chem.* **63**, 635 (2012).
- [6] A. Palacios, D. A. Horner, T. N. Rescigno, and C. W. McCurdy, Two-photon double ionization of the helium atom by ultrashort pulses, *J. Phys. B* **43**, 194003 (2010).

- [7] A. A. Sorokin, M. Wellhöfer, S. V. Bobashev, K. Tiedtke, and M. Richter, X-ray-laser interaction with matter and the role of multiphoton ionization: Free-electron-laser studies on neon and helium, *Phys. Rev. A* **75**, 051402 (2007).
- [8] Hirokazu Hasegawa, Eiji J. Takahashi, Yasuo Nabekawa, Kenichi L. Ishikawa, and Katsumi Midorikawa, Multiphoton ionization of He by using intense high-order harmonics in the soft-x-ray region, *Phys. Rev. A* **71**, 023407 (2005).
- [9] Philippe Antoine, Emmanuel Fomouuo, Bernard Piraux, Toshihiko Shimizu, Hirokazu Hasegawa, Yasuo Nabekawa, and Katsumi Midorikawa, Two-photon double ionization of helium: An experimental lower bound of the total cross section, *Phys. Rev. A* **78**, 023415 (2008).
- [10] M. W. McIntyre, A. J. Kinnen, and M. P. Scott, Photo-double-ionization of the He and Be isoelectronic sequences within an intermediate-energy R-matrix framework, *Phys. Rev. A* **88**, 053413 (2013).
- [11] M. S. Pindzola, C. P. Ballance, Sh. A. Abdel-Naby, F. Robicheaux, G. S. J. Armstrong, and J. Colgan, Single and double photoionization of Be and Mg, *J. Phys. B* **46**, 035201 (2013).
- [12] D. C. Griffin, M. S. Pindzola, C. P. Ballance, and J. Colgan, Double photoionization of Be and Mg atoms using the R-matrix-with-pseudostates method, *Phys. Rev. A* **79**, 023413 (2009).
- [13] S. Laulan and H. Bachau, One- and two-photon double ionization of beryllium with ultrashort ultraviolet laser fields, *Phys. Rev. A* **69**, 033408 (2004).
- [14] M. Kurka, A. Rudenko, L. Foucar, K. U. Kühnel, Y. H. Jiang, Th. Ergler, T. Havermeier, M. Smolarski, S. Schössler, K. Cole, M. Schöffler, R. Dörner, M. Gensch, S. Düsterer, R. Treusch, S. Fritzsche, A. N. Grum-Grzhimailo, E. V. Gryzlova, N. M. Kabachnik, C. D. Schröter, R. Moshhammer, and J. Ullrich, Two-photon double ionization of Ne by free-electron laser radiation: A kinematically complete experiment, *J. Phys. B* **42**, 141002 (2009).
- [15] E. P. Benis, D. Charalambidis, T. N. Kitsopoulos, G. D. Tsakiris, and P. Tzallas, Two-photon double ionization of rare gases by a superposition of harmonics, *Phys. Rev. A* **74**, 051402(R) (2006).
- [16] P. Tzallas, E. Skantzakis, L. A. A. Nikolopoulos, G. D. Tsakiris, and D. Charalambidis, Extreme-ultraviolet pump @ Sprobe studies of one-femtosecond-scale electron dynamics, *Nat. Phys.* **7**, 781 (2011).
- [17] D. A. Horner, F. Morales, T. N. Rescigno, F. Martin, and C. W. McCurdy, Two-photon double ionization of helium above and below the threshold for sequential ionization, *Phys. Rev. A* **76**, 030701 (2007).
- [18] F. L. Yip, C. W. McCurdy, and T. N. Rescigno, Hybrid orbital and numerical grid representation for electronic continuum processes: Double photoionization of atomic beryllium, *Phys. Rev. A* **81**, 053407 (2010).
- [19] F. L. Yip, C. W. McCurdy, and T. N. Rescigno, Double photoionization of excited lithium and beryllium, *Phys. Rev. A* **81**, 063419 (2010).
- [20] F. L. Yip, F. Martín, C. W. McCurdy, and T. N. Rescigno, Double *k*-shell photoionization of atomic beryllium, *Phys. Rev. A* **84**, 053417 (2011).
- [21] A. Palacios, C. W. McCurdy, and T. N. Rescigno, Extracting amplitudes for single and double ionization from a time-dependent wave packet, *Phys. Rev. A* **76**, 043420 (2007).
- [22] A. Palacios, T. N. Rescigno, and C. W. McCurdy, Cross sections for short-pulse single and double ionization of helium, *Phys. Rev. A* **77**, 032716 (2008).
- [23] F. L. Yip, A. Palacios, T. N. Rescigno, C. W. McCurdy, and F. Martín, Time-dependent formalism of double ionization of multielectron atomic targets, *Chem. Phys.* **414**, 112 (2013).
- [24] J. Colgan and M. S. Pindzola, Double photoionization of beryllium, *Phys. Rev. A* **65**, 022709 (2002).
- [25] T. N. Rescigno and C. W. McCurdy, Numerical grid methods for quantum-mechanical scattering problems, *Phys. Rev. A* **62**, 032706 (2000).
- [26] C. W. McCurdy, M. Baertschy, and T. N. Rescigno, Solving the three-body Coulomb breakup problem using exterior complex scaling, *J. Phys. B* **37**, R137 (2004).
- [27] T. N. Rescigno, M. Baertschy, and C. W. McCurdy, Resolution of phase ambiguities in electron-impact ionization amplitudes, *Phys. Rev. A* **68**, 020701 (2003).
- [28] Emmanuel Fomouuo, Gérard Lagmago Kamta, Gaston Edah, and Bernard Piraux, Theory of multiphoton single and double ionization of two-electron atomic systems driven by short-wavelength electric fields: An *ab initio* treatment, *Phys. Rev. A* **74**, 063409 (2006).
- [29] Vicente Hernandez, Jose E. Roman, and Vicente Vidal, SLEPc: A scalable and flexible toolkit for the solution of eigenvalue problems, *ACM Trans. Math. Software* **31**, 351 (2005).
- [30] V. Hernandez, J. E. Roman, A. Tomas, and V. Vidal, *A Survey of Software for Sparse Eigenvalue Problems*, Tech. Rep. STR-6 (Universitat Politècnica de València, 2009), available at <http://www.grycap.upv.es/slep>.
- [31] Satish Balay, Shrirang Abhyankar, Mark F. Adams, Jed Brown, Peter Brune, Kris Buschelman, Victor Eijkhout, William D. Gropp, Dinesh Kaushik, Matthew G. Knepley, Lois Curfman McInnes, Karl Rupp, Barry F. Smith, and Hong Zhang, PETSc Web page, <http://www.mcs.anl.gov/petsc> (2014).
- [32] H. Bachau and P. Lambropoulos, Theory of the photoelectron spectrum in double ionization through two-photon absorption from $he(2s^2)$, *Phys. Rev. A* **44**, R9 (1991).
- [33] J. Feist, S. Nagele, R. Pazourek, E. Persson, B. I. Schneider, L. A. Collins, and J. Burgdörfer, Probing Electron Correlation via Attosecond Xuv Pulses in the Two-Photon Double Ionization of Helium, *Phys. Rev. Lett.* **103**, 063002 (2009).
- [34] A. Palacios, T. N. Rescigno, and C. W. McCurdy, Time-dependent treatment of two-photon resonant single and double ionization of helium by ultrashort laser pulses, *Phys. Rev. A* **79**, 033402 (2009).
- [35] Dae-Soung Kim, Swaraj S. Tayal, Hsiao-Ling Zhou, and Steven T. Manson, Photoionization of atomic beryllium from the ground state, *Phys. Rev. A* **61**, 062701 (2000).
- [36] C. Y. Lin and Y. K. Ho, Influence of debye plasmas on photoionization of li-like ions: Emergence of cooper minima, *Phys. Rev. A* **81**, 033405 (2010).
- [37] G. Peach, H. E. Saraph, and M. J. Seaton, Atomic data for opacity calculations. ix. the lithium isoelectronic sequence, *J. Phys. B* **21**, 3669 (1988).
- [38] J. Feist, R. Pazourek, S. Nagele, E. Persson, B. I. Schneider, L. A. Collins, and J. Burgdörfer, Electron correlation in two-photon double ionization of helium from attosecond to XFEL pulses, *J. Phys. B* **42**, 134014 (2009).